# Basic Characteristics of a Consequent-Pole Type Bearingless Motor

Jun Amemiya, Akira Chiba, *Senior Member*, *IEEE*
David G Dorrell, *Member, IEEE* and Tadashi Fukao, *Fellow*, *IEEE*

***Abstract* --- In this paper, the basic characteristics of a consequent-pole bearingless motor are described. The consequent-pole type rotor has buried permanent magnets polarized in the same radial direction. An analysis is carried out to find the optimum pole number for the machine to produce stable magnetic suspension. The results indicate that there is decoupling of the radial suspension forces from the drive torque when eight or more poles are used. A comparison is given for the torque and suspension force generation with respect to a conventional surface-mount PM rotor. It is shown that the suspension force is several times higher for the consequent-pole rotor; however the torque decreases by 12%. A test machine was built and the torque and suspension characteristics were confirmed. Comparison is also made with other conventional bearingless motors.**

***Index Terms* --- bearingless motor, magnetic bearing, PM motor, consequent-pole.**

## I. Introduction

Recently various bearingless motors (motors that have electro-magnetic integration of the magnetic bearing and the motor drive) have been developed in several countries. For the permanent magnet bearingless motor, a variety of types and topologies have been proposed, e.g., the surface mounted permanent magnet motor (SPM) [1]-[7], the inset permanent magnet motor [8], the buried permanent magnet motor (BPM) [9]-[11], the interior permanent magnet motor (IPM), the homopolar hybrid motor [12][13], etc. However most of these permanent magnet bearingless motors need rotor angular position sensing for feedback to the magnetic suspension controller as well as radial position sensing. This is because if the angular position of the field has a significant error the magnetic suspension loop may not be stable. However in homopolar and hybrid motors the magnetic suspension controller does not need the exact angular position of magnetic field. All these bearingless motors have two rotors in tandem so that they are suitable for 4-axis active magnetic suspension.

To produce 2-axis magnetic suspension the authors have proposed a consequent-pole type of bearingless motor [14]. The proposed machine has the original structure of a consequent-pole permanent magnet rotor, which is still rarely used because they do not offer an advantage in terms of a standard motor drive. However they do offer a significant advantage in terms of a bearingless drive system. One of the advantages is that the suspension force is generated by dc current in a similar manner to the homopolar and hybrid PM motors. Also thick permanent magnets can be used for both torque and suspension force generation so that high torque and suspension force are theoretically possible. However the pole number selection, with verification via test results and comparisons, has not yet been reported.

In this paper, a suspension force analysis of a consequent-pole motor is presented to highlight the importance of pole number selection. A prototype test machine is built and tested and the suspension force is measured. The characteristics of motor performance under the torque load are examined. It is found that amongst the selection of rotors used in bearingless machines, the consequent-pole rotor is superior in both suspension force and torque generation.

Manuscript received February 22, 2004; revised May 28,2004.

Jun Amemiya and Akira Chiba are with Department of Electrical Engineering, Tokyo University of Science, 2641 Yamazaki, Noda, Chiba 278-8510, Japan (e-mail: chiba@ee.noda.tus.ac.jp).

David G Dorrell is with Department of Electronics and Engineering, University of Glasgow, G12 8LT, UK (e-mail: d.dorrell@elec.gla.ac.uk). He was with the Tokyo University of Science in September, 2002.

Tadashi Fukao is with Department of Mechanical Systems Engineering, Faculty of Technology, Musashi Institute of Technology, Japan.

## II. Principle of Suspension Force Generation

Fig. 1 shows the rotor cross section of a consequent-pole bearingless motor. The permanent magnets are magnetized in the same radial direction so that magnet flux has to circulate round through the iron poles between the permanent magnets. Thus, the iron poles are consequently magnetized as S-poles. Therefore, this motor is known as a consequent-pole motor [15]. This motor has 8-poles: four permanent magnet poles and four consequently magnetized iron poles.

In this type of motor the principle of suspension force generation is different from the conventional PM bearingless motor. Fig. 2(a) shows the principle of suspension force

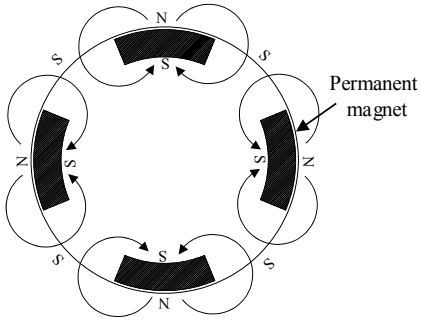


Fig. 1. Consequent-pole type rotor.

generation.

$N_x$ and $N_y$ indicate suspension conductors in a stationary coordinate system. The dominant 8-pole flux $\Psi_m$ is generated by the permanent magnets; and in addition a 2-pole suspension flux $\Psi_x$, generated by the current in the conductors $N_x$, is superimposed upon it. In the airgap under the iron-poles of the right-hand half of the motor the flux density is increased as indicated by "dense". However, in the left-hand half the flux density is decreased as indicated by "sparse". Therefore, a positive suspension force is generated in the horizontal $x$-axis direction. Hence the suspension force is generated by an interaction between the permanent magnet flux and the suspension-winding current flux. Fig. 2(b) shows a rotor at an angular position of 45° (mech). The flux density under the right-hand iron pole increases while under the left-hand iron pole it decreases. Therefore the suspension force is still generated in the $x$-axis direction. Hence the direction of suspension force is independent of the rotor angular position. The suspension force is almost proportional to the $N_x$ winding current and negative current will generate negative $x$-axis force. In a similar manner, the $N_y$ winding current generates $y$-axis suspension force. The total suspension force is generated by a vector sum of the $x$- and $y$-axis forces.

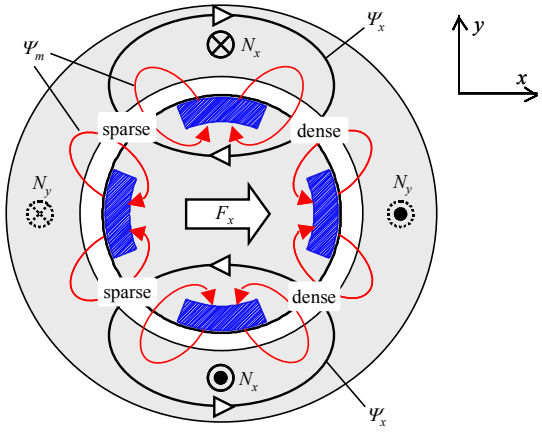


(a) Rotor angle $\phi$=0deg

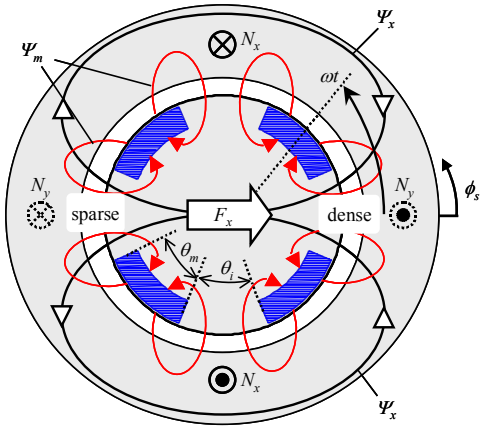


$\Psi_m$: 8-pole PM flux path
$\Psi_x$: 2-pole flux path
(b) Rotor angle $\phi$=45deg

Fig. 2. Principle of suspension force generation

## III. Magnetic Suspension and Rotor Poles

In this section, an analytical analysis for the calculation of the suspension force is put forward and calculated from airgap flux density distribution using the assumptions specified below

- The magnetic circuit is linear
- The rotor is centered
- Suspension and motor winding MMFs are sinusoidally distributed
- Only $x$-axis suspension MMF is considered for simplicity
- The PMs are thick, thus force is generated only under the iron rotor poles
- The stator permeance is uniform (i.e., no stator saliency or slotting)
- Airgap flux flows in the radial direction only

Note that the influence of non-sinusoidal MMF distribution on suspension force is described in reference [14,16].

Fig. 2(b) shows the parameter and coordinate definitions. $\theta_m$ and $\theta_i$ are the magnet and iron pole arcs (in radians). $\phi_s$ is the stator angular coordinate, and $\omega t$ is rotor rotational position at time $t$.

The flux under the rotor iron pole is composed of the PM flux and flux produced by the suspension and motor windings. Therefore the total MMF can be represented as

$$A(\phi_s) = A_P + A_{sx}\cos(\phi_s) + A_m \sin[p(\phi_s - \omega t)] \qquad (1)$$

where:

$A_p$ is the component of airgap MMF due to the permanent magnet
$A_{sx}$ is the component of MMF due to current in the suspension winding $N_x$
$A_m$ is the component of MMF due motor winding current
$p$ is the rotor pole-pair number

Next, let us derive the airgap flux density. Fig. 3 shows a mathematical representation of permeance distribution along the stator angular coordinate $\phi_s$. A square waveform for the permeance is assumed; with the iron-rotor pole having amplitude $P_i$ so that

$$P_i = 2\pi r l \mu_0 / g \qquad (2)$$

where $g$ is the airgap length, $r$ is the mean airgap radius, $l$ is the stack length, and $\mu_0$ is the permeability of free space. The airgap flux $\Psi$ for $d\phi_s$ is given as a product of $P_i$, $A(\phi_s)$ and $d\phi_s/2\pi$ where

$$\Psi = r l \mu_0 A(\phi_s) d\phi_s / g \qquad (3)$$

Hence the airgap flux density $B_g(\phi_s)$ is obtained from the airgap-flux divided by an area $rld\phi_s$:

$$B_g(\phi_s) = \frac{\mu_0}{g} A(\phi_s) \tag{4}$$

The magnetic force d$F$ generated over a small angular airgap section d$\phi_s$ can be obtained from the Maxwell stress:

$$\mathrm{d}F = \frac{lr}{2\mu_0} B_g{}^2(\phi_s)\mathrm{d}\phi_s \tag{5}$$

The vector integration of the stress force in the $x$-axis results in total magnetic force $F_x$ where

$$F_x = \frac{lr}{2\mu_0}\int_0^{2\pi} B_g{}^2(\phi_s)\cos(\phi_s)\mathrm{d}\phi_s \tag{6}$$

In Fig. 3, the permeance distribution has $p$ square pole-pieces of span $\theta_i$ which correspond to the rotor iron poles. Between these pole-pieces are the permanent magnet poles, where the permeance is assumed to be zero. Note that a stress force does exist in PM region of the airgap; however, in the radial stress integration (6) it is assumed to be zero because of the flux flowing through the magnets which is sourced from the 2-pole winding is negligible. For the $k$-th pole, a permeance exists between $\omega t+\theta_m+2\pi(k\text{-}1)/p$ and $\omega t\text{-}\theta_m/2+2\pi k/p$. An integration of the stress force in this area provides a suspension force which can be vectorized along either the $x$-axis or $y$-axis. The summation of the $x$-axis forces for 1 to $p$ pole-pieces results in $F_x$. Substituting (4) into (6) and considering the summation and the integration gives $F_x$ as

$$F_x = \frac{\mu_0 lr}{2g^2}\sum_{k=1}^{p}\int_{\omega t+\frac{\theta_m}{2}+\frac{2\pi}{p}(k-1)}^{\omega t-\frac{\theta_m}{2}+\frac{2\pi}{p}k} A^2(\phi_s)\cos(\phi_s)\mathrm{d}\phi_s \tag{7}$$

The $y$-axis force is obtained in the similar way:

$$F_y = \frac{\mu_0 lr}{2g^2}\sum_{k=1}^{p}\int_{\omega t+\frac{\theta_m}{2}+\frac{2\pi}{p}(k-1)}^{\omega t-\frac{\theta_m}{2}+\frac{2\pi}{p}k} A^2(\phi_s)\sin(\phi_s)\mathrm{d}\phi_s \tag{8}$$

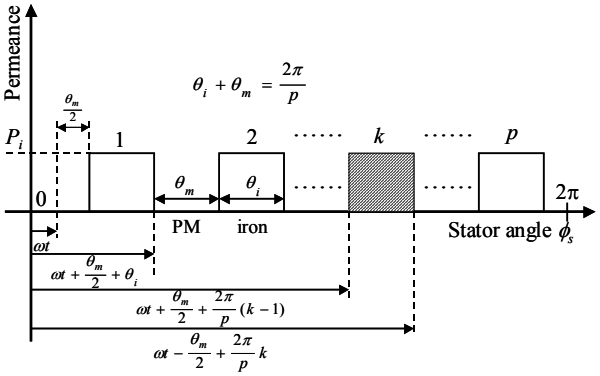


Fig. 3. Permeance distribution

When $p = 2$, the integrals (7) and (8) become

$$F_x = -\frac{\mu_0 lr}{4g^2} A_{sx}\{4A_p[-\pi+\cos(2\omega t)\sin(\theta_m)+\theta_m] + A_m\sin(2\omega t)[2\pi+\sin(2\theta_m)-2\theta_m]\} \tag{9}$$

$$F_y = \frac{\mu_0 lr}{4g^2} A_{sx}\{-4A_p\sin(\theta_m)\sin(2\omega t) + A_m\cos(2\omega t)[2\pi+\sin(2\theta_m)-2\theta_m]\} \tag{10}$$

This equation produces unwanted (vibration) terms when $p$ = 2 and also the motor winding current term $A_m$ is included. Hence motor torque current interferes with the suspension force and also the term $\omega t$ means that the suspension force is dependent on the rotor rotational position producing vibration components. In addition, $F_y$ is not zero despite the fact that we are attempting to produce force along the $x$-axis only.

If $p$ = 3, the integrals (7) and (8) are simplified to

$$F_x = -\frac{\mu_0 lr}{4g^2} A_{sx}[A_{sx}\sin(\frac{3}{2}\theta_m)\cos(3\omega t)+A_p(-4\pi+6\theta_m)] \tag{11}$$

$$F_y = -\frac{\mu_0 lr}{4g^2} A_{sx}{}^2\sin(\frac{3}{2}\theta_m)\sin(3\omega t) \tag{12}$$

The term $A_m$ disappears. However, there remains the term $\omega t$ which will still generate vibration in both the $x$- and $y$-axis directions.

If $p \geqq 4$ the integrals simplify even further so that

$$F_x = \frac{\mu_0 lr}{2g^2} A_p A_{sx}(2\pi - p\theta_m) \tag{13}$$

$$F_y = 0 \tag{14}$$

Hence the terms $A_m$ and $\omega t$ disappear so that a suspension force is generated which is independent of torque current and rotor rotational position and which is orientated along the $x$-axis only. Hence an $x$-axis suspension force only is generated by the $N_x$ winding current. Since the $x$-axis and $y$-axis structures are symmetrical, only a $y$-axis suspension force is generated by the $N_y$ winding current. Therefore it is found that the suspension forces are now inherently decoupled when the pole-pair number is 4 or more.

This analysis is analytical and has several approximations. The main approximations are the assumption of zero permeance under the permanent magnet poles for the flux produced by the 2-pole suspension winding and also the assumption of sinusoidal MMF distribution produced by the motor and suspension windings. A paper that gives an alternative analysis technique was recently published [16] and this uses rotating field theory to illustrate the effect of the MMF winding harmonics on the force. It was found that the 5th, 7th, 11th, 13th, etc, winding harmonics of both the motor and suspension windings can lead to parasitic vibrations of varying frequency however these are small if the winding is well designed and this was illustrated by finite element analysis.

Fig. 4 shows finite element analysis results using the *SPEED* PC-FEA program from The University of Glasgow, UK. A static analysis is carried out over 90 rotor rotational positions for symmetry. DC current is supplied to distributed conductors representing the $N_x$ winding which has a distributed 3-phase layout in the 24 slots stator. The MMF vector produced by the 3-phase DC currents is along the $x$-axis. The motor current is zero so that $A_m$ is zero. The PM

and iron arcs $\theta_m$ and $\theta_i$ are both $\pi/p$. The following correspondence between equations (9) to (14) and the FEM results of Fig. 4 can be observed:

(i) When $p$ = 2 and there is no motor winding current, the second term in (9) simplifies to zero and a twice rotational-speed oscillation is occurred by the first term which is a negative cosine wave. This can be observed in $F_x$ where it halves a negative cosine wave oscillating around a constant offset. For quarter rotation this is correct. Under the same conditions (10) simplifies to a twice rotational-speed oscillation in the first term which is a negative sine wave which $F_y$ agrees with.

(ii) When $p$ = 3, according to (11) and (12), $F_x$ and $F_y$ should have an oscillation component which is three times the rotational speed, i.e., we should see an oscillation with ¾ of a cycle. However when comparing the coefficients in (11) we will see that $4\pi A_p$ ($A_p$ being the magnet MMF) is likely to be much higher than $A_{sx}\sin(3\theta_m/2)$ (the suspension current MMF in the along the $x$-axis) and in this case this appears to be so. However if the motor was designed with thinner magnets and a larger airgap it could well be that the difference between the coefficients is less and the oscillation becomes more marked.

(iii) When $p$ = 4 some force oscillation still exists. These variations are caused by MMF harmonics and stator teeth permeance variations, which are neglected in the above analytical equations. The MMF harmonic contribution was described in [16].

It can be concluded that, while a pole-pair number of 3 for the rotor may well be operated successfully, the theory suggests that the number of rotor pole pairs should be selected to be four or more, otherwise some designs may well produce force oscillations.

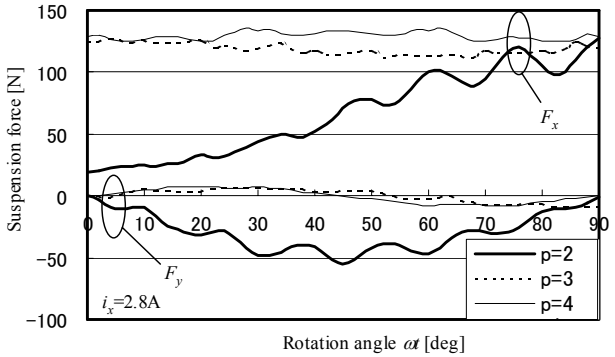


Fig. 4. Suspension force analysis (PC-FEA)

## IV. Torque and Force Comparison

In this section, the torque and suspension force capabilities of a consequent-pole type rotor are compared to similar 8-pole buried permanent magnet (BPM) and 4-pole BPM rotors, using PC-FEA. Torque generation is compared with the 8-pole BPM rotor (having an identical stator) under

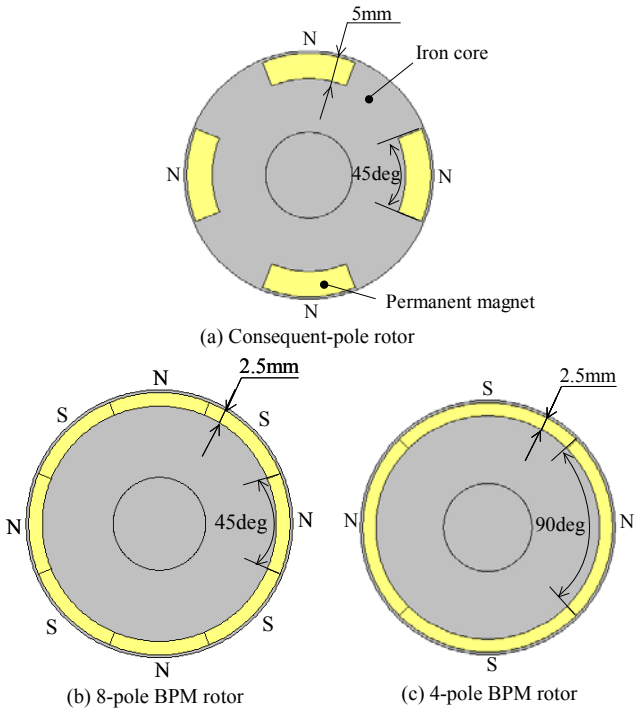


Fig.5. Analysis model

similar current conditions. Suspension force cannot be compared with the 8-pole BPM rotor because no suspension force can be generated with 2-pole stator windings. Thus, a 4-pole BPM rotor machine is used for radial force comparison. Fig. 5 shows cross-sections of the three rotors. The BPM may resemble a surface magnet rotor except there is a steel layer over the magnet surface to retain the magnets on the rotor. There may also be $q$-axis saliency due to the inter-pole steel web which retains the steel surface layer. The stator core and windings are the same as the prototype machine described in later sections. The PM thickness was chosen so that the amount of permanent magnet volume material is identical.

Fig. 6 compares the torque between the two 8-pole rotors of (a) and (b) under an identical current condition. The stator winding is an 8-pole winding in 24 slots. Therefore this winding has one coil per pole per phase, which is usually a winding strategy for brushless DC (square wave current) control. However we are using brushless AC (sine wave current) control; but it is quite common to use a brushless DC machine in a brushless AC application and vice versa with the penalty of torque ripple. Hence the torque ripple presented in Fig. 6 is not a problem at this stage and quite common in some drive systems with high inertia. The average torque for the BPM is 2.57 Nm and for the consequent-pole machine it is 2.3 Nm. The current in both cases is 7.8 A which is on the rotor $q$-axis. 8-pole BPM torque is about 12% higher so that the torque values are quite close. Fig. 7 shows the flux line and tooth flux density under torque load. The flux density in the 8-pole BPM is higher than consequent-pole by few percent on the $q$-axis.

Fig. 8 shows a comparison of the suspension force between the two cases of (a) and (c) in Fig 5. Note that the 4-pole BPM suspension current is ac sine-wave current. The average suspension force for consequent-pole machine was 130 N whereas for the 4-pole BPM it was only 37 N. Thus, the consequent-pole generates 3.5 times more suspension force.

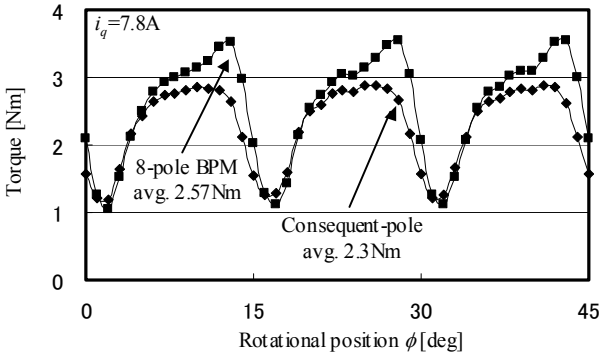


Fig.6. Torque comparison

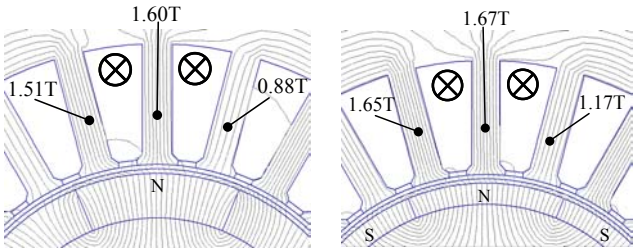


(a) Consequent-pole (b) 8-pole BPM

Fig.7. Comparison of flux lines under torque load ($i_q$=7.8A)

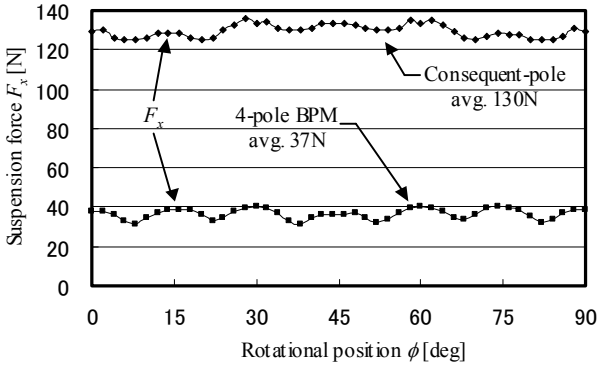


Fig.8. Suspension force comparison

**TABLE I**

MOTOR PARAMETERS

| | |
|---|---|
| Stator outer diameter | 95mm |
| Stator bore | 50mm |
| Stator slot | 24 |
| Motor winding | 8-pole 3-phase |
| Suspension winding | 2-pole 3-phase |
| Rotor diameter | 49mm |
| Rotor type | 8-pole consequent |
| Magnet thickness | 5mm |
| Magnet arc | 45deg |
| Remanent magnetism | 1.3T |
| Airgap length | 0.5mm |
| Stack length | 50mm |

The suspension force is found to be significant in the consequent-pole rotor machine thanks to the high permeance under the iron rotor poles where the suspension force is generated, as described in a previous section.

## V. Experimental Results

### A. Prototype Machine

A prototype consequent-pole machine was constructed to verify the theory and the specification of the machine is listed in Table I.

Fig.9 shows a photograph of the prototype machine. At the top of the machine there are two eddy-current type gap sensors in *x*- and *y*-axes. The bottom of the shaft is supported by a mechanical bearing so that this machine has two axes of freedom. In a full bearingless drive system there would be one control and gap sensors at each end of the shaft for 4 axes of freedom and complete magnetic suspension (a magnetic thrust bearing may also be used). Therefore this represents half of a bearingless drive unit and is quite suitable for the experiments carried out here. A jig for a weight-hang test is also shown. In this jig, a weight is hung by a wire, which is attached to the shaft via a bearing and a pulley arrangement orientated along the negative *x*-axis so that the test machine has to generate a suspension force in positive *x*-axis direction to counteract the force from the weight. The value of suspension force is given by

$$F = m \times 9.807[m/s^2] \times 2.18 \qquad (15)$$

where $F$ is suspension force [N], $m$ is the weight [kg] and 2.18 is a lever coefficient which is the ratio of the height of the wire attachment to the height of the axial centre of the machine above the mechanical bearing – essentially we are taking moments round the bottom mechanical bearing. In this case the weight is 6 kg so that generated suspension force is about 130 N.

Fig. 10 shows the system configuration of the prototype machine. The upper part of the block diagram shows the motor controller block. The speed is controlled by a PI controller which has the error between the speed reference and the actual speed fed into it. The rotor speed is detected by a rotary encoder. This system is standard for a brushless AC PM drive.

The lower side shows the suspension controller block. The displacements *x* and *y* are detected by the gap sensors. The detected displacement errors are amplified in the PID controllers so that the suspension current commands, which are in 2-phase coordinates, are transformed into 3-phase. The inverter is controlled by the 3-phase current commands and supplies the suspension winding currents. Note that rotor angular position feedback is not required in the suspension controller unlike most bearingless motor suspension systems. This is one of the main advantages of this sort of bearingless drive suspension control.

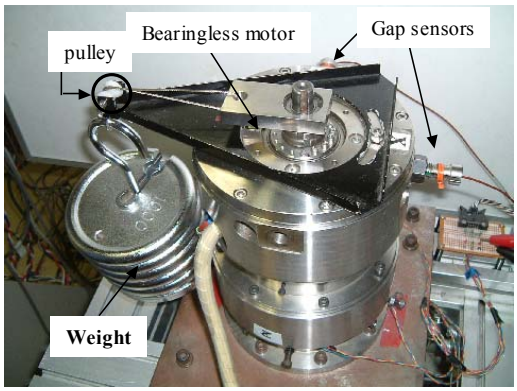


Fig. 9. Prototype machine

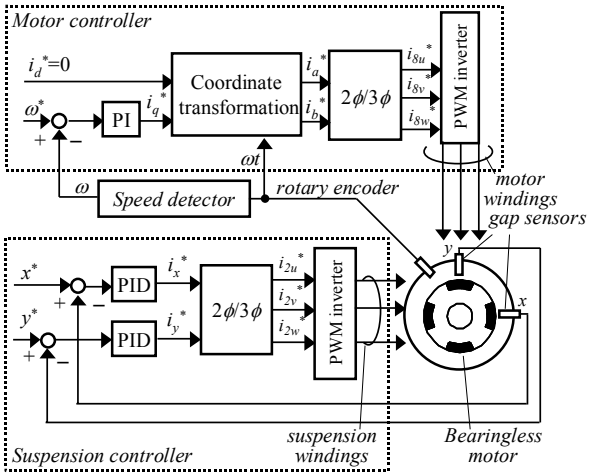


Fig. 10. System configuration

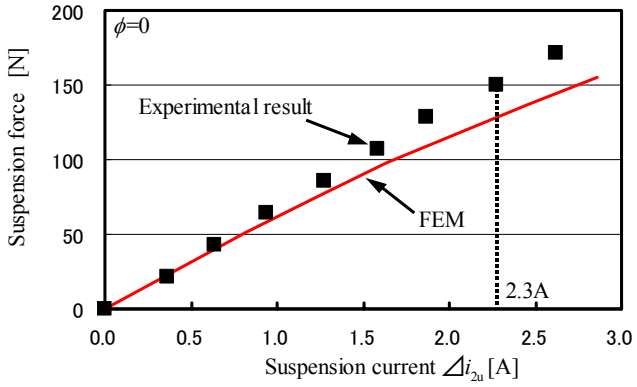


Fig. 11. Suspension force at stand still

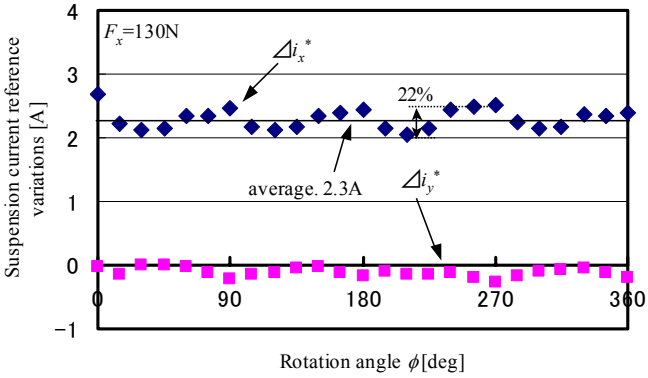


Fig.12. Suspension current reference and rotor rotational position

## B. *Experimental results from the prototype machine.*

Fig. 11 shows a comparison between the measured suspension force along the *x*-axis and FEM analysis at stand still. This figure shows an increase of *u*-phase suspension current $\Delta i_{2u}$ (which corresponds to the *x*-axis) versus suspension force. At the rated value of $\Delta i_{2u}$, a suspension force of about 150 N was generated. This result confirms suspension force generation in Fig. 8 shown in the previous section. The agreement is fair although there is about 15 % error under high load with the suspension force being underestimated. This could be for a number of reasons. Static friction in the pulley system will leads to a measurement that is higher that the actual force. End effects in the motor (which are not modeled in 2D FEA), tolerance variation in construction (especially around airgap and PM area), and material and temperature variation in the analysis (such as magnets modeled with a lower $B_r$ than actually present) will also give inaccuracy. The suspension force is very susceptible to variations because it is due to the vector summation of the small differences in the airgap flux density on opposite sides on the airgap diameter.

Fig. 12 shows the rotor angular position $\phi$ versus the required suspension currents references $\Delta i_x^*$ and $\Delta i_y^*$ while the *x*-axis suspension force is kept constant at 130 N. If the suspension force is truly independent of $\phi$ then $\Delta i_x^*$ should be constant and $\Delta i_y^*$ should be zero. However, as can be seen from Fig 12, the suspension force is not totally independent of $\phi$, as previously shown in Fig. 4; but $\Delta i_x^*$ and $\Delta i_y^*$ are automatically generated by the suspension feedback loops so that they can compensate for the 22% force variation to produce stable operation. In a conventional bearingless motor, $\Delta i_x^*$ is a cosine function of $\phi$ and $\Delta i_y^*$ is a sine function (i.e, the suspension winding current is a rotating vector) with similar slight fluctuations from the ideal. In comparison, here it can be seen that suspension force is almost independent of a rotor angular position and almost self aligning so that the control problem is a much easier task, as stated earlier.

Fig. 13 shows the experimental system for the torque load tests. The motor is driven by a PWM voltage source inverter. A digital power meter detects the *rms* voltage, current and input power to the motor. The shaft torque and speed are detected by a torque transducer and a DC generator and load resistance are connected as a shaft load. One of the prime interests is to find out if the consequent-pole motor can realize the same shaft output as standard SPM motor. Fig 14 shows the variation of shaft output power with motor current at three different speeds for the experimental machine. The maximum output power is 929 W at 4000 r/min. Fig. 15 gives the corresponding torque characteristics which illustrates that the torque is a function of motor current and has little dependency on speed. This also shows very low

speed-dependant windage and friction losses and low iron losses. The maximum torque value is 2.2 Nm. Table II summarizes the load test results at 4000 r/min. The output is 5% lower with respect to the FEM result because of iron and mechanical loss; however, this is reasonable, and the torque is as high as expected.

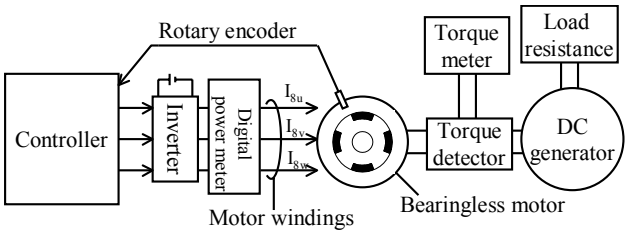


Fig. 13. Motor load test setup

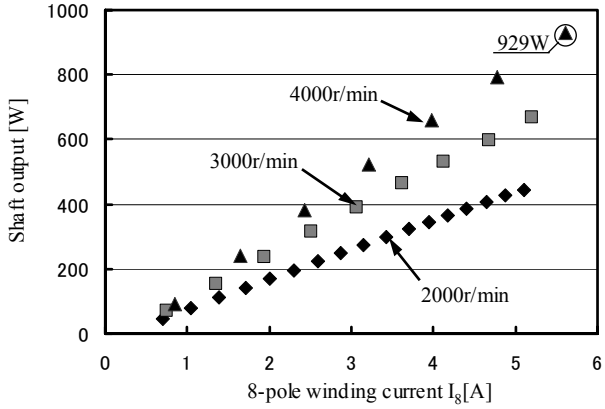


Fig 14. Shaft output characteristics

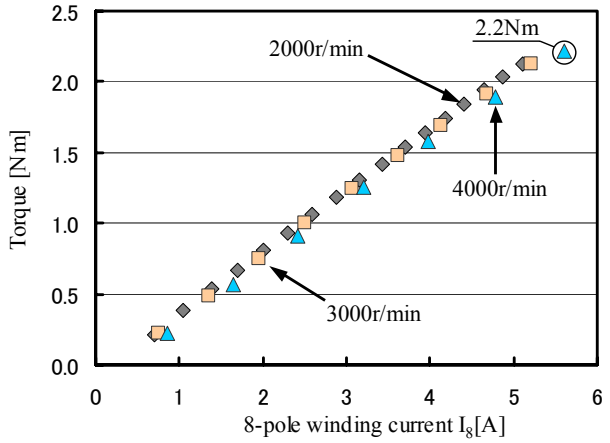


Fig 15. Torque characteristics

**TABLE II**
LOAD TEST RESULTS

| | |
|---|---|
| Rotational speed | 4000r/min |
| 8-pole line current | 5.6A |
| Line to line voltage | 145V |
| Input power | 1091W |
| Shaft output | 929W |
| Copper loss | 90W |
| Iron loss and mechanical loss | 72W |
| Torque | 2.2Nm |
| Efficiency | 85.1% |
| Power factor | 0.78 |

### *C. Comparison of motor performance*

In this section the experimental results of the consequent-pole type bearingless motor are compared, in terms of suspension force and torque, with two other types of bearingless PM motors that have been previously built and tested. These machines are a BPM motor [11] and an inset type of motor [8]. In Table III, the maximum suspension force is divided by the rotor diameter $D$ and stack length $L$. For the torque comparison, it is divided by $D^2$ and $L$. Remember that the suspension force is the vector integration of the radial stress around the airgap while the torque is the mean airgap radius multiplied by the integration of the tangential stress around the airgap. Hence the different normalizations - the suspension force is normalized with respect to an arbitrary rotor surface area whereas the torque is normalized to an arbitrary rotor volume. In a conventional BPM bearingless motor, there is a trade-off between the suspension force and torque. In the prototype BPM used in Table III, the suspension force is high whereas the torque is low. There is a similar trade-off for the inset type of machine and in this instance the torque is designed to be high and the suspension force low. However the consequent-pole type has both high suspension force and torque. In other words, the consequent-pole type bearingless motor avoids the trade-off so that it can achieve high performance in both suspension force and torque.

**TABLE III**
COMPARISON MOTOR PERFORMANCE

| Rotor type | Suspension force/$DL$ [$10^3$N/m$^2$] | Torque/$D^2L$ [$10^4$N/m$^2$] |
|---|---|---|
| Consequent-pole | 61.2 | 1.77 |
| BPM | 55.7 | 0.76 |
| Inset | 5.7 | 1.78 |

## VI. CONCLUSIONS

In this paper, we have introduced the basic characteristics of a consequent-pole type bearingless motor. It has been shown that stable radial suspension force can be generated when the rotor has eight or more poles. The suspension feedback controller is simplified because rotor angular position feedback is not required, which is unlike most bearingless motor drives.

In the experimental results, it is shown that the consequent-pole test machine can achieve high torque and force simultaneously for given currents. The machine is therefore free from force and torque trade-off when compared to conventional PM bearingless motors.

If the torque and suspension MMFs are quite high, there is a decrease in suspension force and also an error in the angular direction of the suspension force is generated. The machine should be designed to avoid this by careful consideration of the stator teeth, airgap length, PM thickness, etc. The design procedure for improved operation of these machines will be reported in future publications.

## VII. REFERENCES


[1] Masahide Ooshima, Satoru Miyazawa, Akira Chiba, Fukuzo Nakamura, Tadashi Fukao, "Performance Evaluation and Test Results of a 11,000r/m, 4kW Surface-Mounted Permanent Magnet-Type Bearingless Motor", ISMB, August 23-25, 2000, ETH Zurich pp. 377-382.

[2] Kousuke Oguri, Masaya Watada, Susumu Torii, Daiki Ebihara, "Design Optimization of Magnetic Bearing Composed of Permanent Magnets for the Bearing-Less Motor", International Symposium on Magnetic Bearings, August 23-25, 2000, ETH Zurich pp. 365-370.

[3] Reto Schoeb, Ntale Barletta, Andreas Fleischli, Giampiero Foiera, Thomas Gempp, H-G.Reiter "A BEARINGLESS MOTOR FOR A LEFT VENTRICULAR ASSIST DEVICE (LVAD)", International Symposium on Magnetic Bearings, August 23-25, 2000, ETH Zurich pp. 383-388.

[4] Yohji Okada, Hirohide Konishi, Hideki Kanebako, Chong-Won Lee, "LORENTZ FORCE TYPE SELF-BEARING MOTOR", International Symposium on Magnetic Bearings, August 23-25, 2000, ETH Zurich pp. 353-358.

[5] Klaus Nenninger, Wolfgang Amrhein, Siegfried Silber, Gernot Trauner, Martin Reisinger. ''MAGNETIC CIRCUIT DESIGN OF A BEARINGLESS SINGLE-PHASE SLICE MOTOR'' 8th International Symposium on Magnetic Bearing, August 26-28 2002, Mito, Japan, pp.265-270.

[6] A.Boletis, R.Vuillemin, C.Aymon, M.Kummerle, B.Aeschlimann, R.Moser, H.Bleuler, E.Fullin, J.Bergqvist, ''A SIX MAGNETIC ACTUATORS INTEGRATED MICROMOTOR'' 7th International Symposium on Magnetic Bearing, August 23-25 2000, *ETH Zurich*, pp.101-103.

[7] Barret Steele, Lyndon Stephens, "A Test Rig for Measuring Force and Torque Production in a Lorenz, Slotless Self Bearing Motor", ISMB, August 23-25, 2000, ETH Zurich pp. 407-412.

[8] Kohei Inagaki, Akira Chiba, M.A.Rahman, Tadashi Fukao, "Performance Characteristics of Inset-Type Permanent Magnet Bearingless Motor Drives", PESWM, 23-27 January 2000 Singapore.

[9] Masahide Ooshima, Satoru Miyazawa, Yusuke Shima, Akira Chiba, Fukuzo Nakamura, Tadashi Fukao, "Increase in Radial Force of A Bearingless Motor with Buried Permanent Magnet-Type Rotor", Proceedings of the Fourth International conference on MOVIC, vol.3, pp. 1077-1082, 1998.

[10] Noriaki Fujie, Rintarou Yoshimatsu, Akira Chiba, Masahide Ooshima, M.A.Rahman, and Tadashi Fukao, "A Decoupling control Method of Buried Permanent Magnet Bearingless Motors considering Magnetic Saturation", IPEC-Tokyo 2000, S-10-6 pp. 395-400.

[11] Masahide Ooshima, Koyu Yamashita, Akira Chiba, M.Azizur Rahman and Tadashi Fukao, "An Improved Control Method of Buried-type IPM Bearingless Motors Considering Magnetic Saturation and Magnetic Pull Variation", IEMDC, June 1-4, 2003, Madison, Wisconsin, USA, pp.1055-1060.

[12] Osamu Ichikawa, Akira Chiba, Tadashi Fukao, "Principles and Structures of Homopolar Type Bearingless Motors", IPEC-Tokyo 2000 pp. 401-406.

[13] Seung-Jong Kim, Tatsunori Shimonishi, Hideki Kanebako, Yohji Okada, "Design of a Hybrid-Type Short-Span Self-Bearing Motor" ISMB, August 23-25, 2000, ETH Zurich pp. 359-364.

[14] Tomohiro Takenaga, Yutaka Kubota, Akira Chiba, Tadashi Fukao, "A PRINCIPLE AND A DESIGN OF A CONSEQUENT-POLE BEARINGLESS MOTOR" 8th International Symposium on Magnetic Bearing, August 26-28 2002, Mito, Japan, pp.259-264.

[15] J.R.Hendershot Jr, T.J.E Miller "Design of Brushless Permanent-Magnet Motors" Oxford Magna Physics 1994.

[16] D. G Dorrell, J. Amemiya, A. Chiba and T. Takenaga "Analytical modelling of a Consequent-Pole Bearingless Permanent Magnet Motor", IEEE Power Electronics and Electric Drives Conference, November 1-5, 2003, Singapore, on CD.



**Jun Amemiya** was born on January 15, 1980 in Chiba prefecture, Japan. He received the B.S degree in electrical engineering from the Tokyo University of Science, in 2003. He is currently working toward the M.S degree. He was with the University of Glasgow in August, 2003.

**Akira Chiba** (S'82-M'88-SM'97) was born in Tokyo, Japan in 1960. He received the BS., MS. and Ph.D. degrees in Electrical Engineering from the Tokyo Institute of Technology, in 1983, 1985 and 1988, respectively.

In 1988, he joined the Science University of Tokyo as a Research Associate in Department of Electrical Engineering in Faculty of Science and Technology. From 1992 to 1993 and from 1993 to 1997 he was Research Lecturer and Senior Lecturer, respectively. He has been Associate Professor since 1997. In 1990, he was an NSERC (Natural Science and Engineering Research Council of Canada) International Post-Doctoral Fellow in the Memorial University of Newfoundland, Canada. He has been studying magnetically suspended bearingless, switched reluctance and super high speed drives. He is a member of IEEJ in Japan and a Senior Member of IEEE.

**David G Dorrell** was born in St Helens, England in 1965. He obtained a BEng degree from The University of Leeds, UK, in 1988 and an MSc degree from The University of Bradford, UK, in 1989. In 1993 he was awarded a PhD degree by The University of Cambridge, UK. His main areas of research are the design and analysis of electric motors and generators, condition monitoring of electric machines and renewable energy applications. He currently holds the post of Senior Lecturer with The University of Glasgow. He is a Chartered Engineer in the UK and a member of the IEE, London and the IEEE.

**Tadashi Fukao** (M'85-SM'93-F'94) was born in Shizuoka Prefecture, Japan in 1940. He received the BS., MS. and Ph.D. degrees in Electrical Engineering from the Tokyo Institute of Technology, in 1964, 1966 and 1969, respectively.

In 1968 he joined the Tokyo Institute of Technology as a Research Associate in the Department of Electrical and Electronic Engineering. From 1977-1986 and from 1986-2001 he was an Associate Professor and a Professor, respectively. In 2001 he joined the Musashi Institute of Technology. He has been a Professor with the Department of Mechanical Systems Engineering. He is engaged in research on high speed motors and bearingless motor drive systems. He is the president of the Institute of Electrical Engineers of Japan from 2003 to 2004.